

Investigation of CO₂ Orientational Dynamics through Simulated NMR Line Shapes**

Patrick Melix^{*[a, b]} and Thomas Heine^[c, d]

The dynamics of carbon dioxide in third generation (i.e., flexible) Metal-Organic Frameworks (MOFs) can be experimentally observed by ¹³C NMR spectroscopy. The obtained line shapes directly correlate with the motion of the adsorbed CO₂, which in turn are readily available from classical molecular dynamics (MD) simulations. In this article, we present our publicly available implementation of an algorithm to calculate NMR line shapes from MD trajectories in a matter of minutes on any current personal computer. We apply the methodology to study an effect observed experimentally when adsorbing CO₂ in

different samples of the pillared layer MOF Ni₂(ndc)₂(dabco) (ndc = 2,6-naphthalene-dicarboxylate, dabco = 1,4-diazabicyclo-[2.2.2]-octane), also known as DUT-8(Ni). In ¹³C NMR experiments of adsorbed CO₂ in this MOF, small (rigid) crystals result in narrower NMR line shapes than larger (flexible) crystals. The reasons for the higher mobility of CO₂ inside the smaller crystals is unknown. Our ligand field molecular mechanics simulations provide atomistic insight into the effects visible in NMR experiments with limited computational effort.

Introduction

For the study of carbon dioxide in solid host systems, ¹³C NMR can be an immensely powerful tool.^[1–4] The chemical shift (δ) of any nucleus per se depends, besides on the structural environment within the molecular structure also on the orientation of the molecule with respect to the external magnetic field. In ideal solutions, this orientational dependence is averaged out ($\bar{\delta}$) due to rapid movement of the species under investigation. This is the reason for the characteristically narrow lines observed in solution NMR experiments. In contrast, this averaging of the chemical shift does not occur in solid state NMR experiments. In these, the species' movement is mostly slower and therefore the anisotropy of the measured signal is retained. The experimental NMR line shapes are therefore directly related to the molecular motion of the CO₂ molecules

in the sample. In simple terms: the more movement the CO₂ molecules exhibit, the narrower the measured line will be. For an overview of the methodology we refer the interested reader to an excellent review by Reimer *et al.*^[2] Commonly, the experimental line shapes are used to fit chemical shift (or shielding) tensors, which can be used to obtain relative positional and motional information about the CO₂ molecules.^[5–7] The opposite route can however also be taken: from molecular dynamics (MD) simulations, the trajectories of the adsorbed CO₂ molecules are readily available. This information can be translated into a residual chemical shift anisotropy (i.e. a chemical shift line width) following two (very similar) previously published methodologies,^[8,9] one of which we implemented in a publicly available Python package.^[10] This simulation-based approach is neither limited to a specific host system, nor to CO₂ as the adsorbate.

Breathing Metal-Organic Frameworks (MOFs),^[11–16] especially in combination with carbon dioxide, have seen a lot of focus over the last years. Investigations into their applicability in e.g. gas sensing, separation and storage have been studied extensively due to the environmental implications of the topic. The pillared layer MOF DUT-8(Ni)^[17] is one of the representatives of this class of materials. It consists of layers of Ni₂(COO)₄ paddle wheels connected by nonlinear ndc (2,6-naphthalene-dicarboxylate) linkers and stacked by pillaring layers with dabco (1,4-diazabicyclo-[2.2.2]-octane). Figure 1 shows a top (along the Ni-dabco-Ni axis) and side view (perpendicular to one half of the ndc linkers) of the structure. One of its remarkable characteristics is the possibility to access two distinct phases by adsorbing guests into/from the structure. After synthesis, the structure is in a solvent-filled open pore state (denoted **op**). Upon solvent removal, it can collapse (unit cell volume changes to less than half the initial volume) into a closed pore state (denoted **cp**). This collapse is, however, not observed if the synthesized crystals are smaller than a certain threshold (approximately 500 nm in length).^[18–20] The size dependence of

[a] Dr. P. Melix
Universität Leipzig
Wilhelm-Ostwald-Institut für Physikalische und Theoretische Chemie
Linnéstraße 2, 04103 Leipzig, Germany
E-mail: patrick.melix@uni-leipzig.de

[b] Dr. P. Melix
Northwestern University
Department of Chemical and Biological Engineering
2145 Sheridan Road, Evanston, Illinois 60208, United States

[c] Prof. T. Heine
TU Dresden, Professur für Theoretische Chemie
Bergstr. 66c, 01062 Dresden, Germany

[d] Prof. T. Heine
Yonsei University
Department of Chemistry
Seodaemun-gu, Seoul 120-749, Republic of Korea

[**] A previous version of this manuscript has been deposited on a preprint server (<https://doi.org/10.33774/chemrxiv-2021-9c33d>).

Supporting information for this article is available on the WWW under <https://doi.org/10.1002/cphc.202100489>

© 2021 The Authors. ChemPhysChem published by Wiley-VCH GmbH. This is an open access article under the terms of the Creative Commons Attribution License, which permits use, distribution and reproduction in any medium, provided the original work is properly cited.

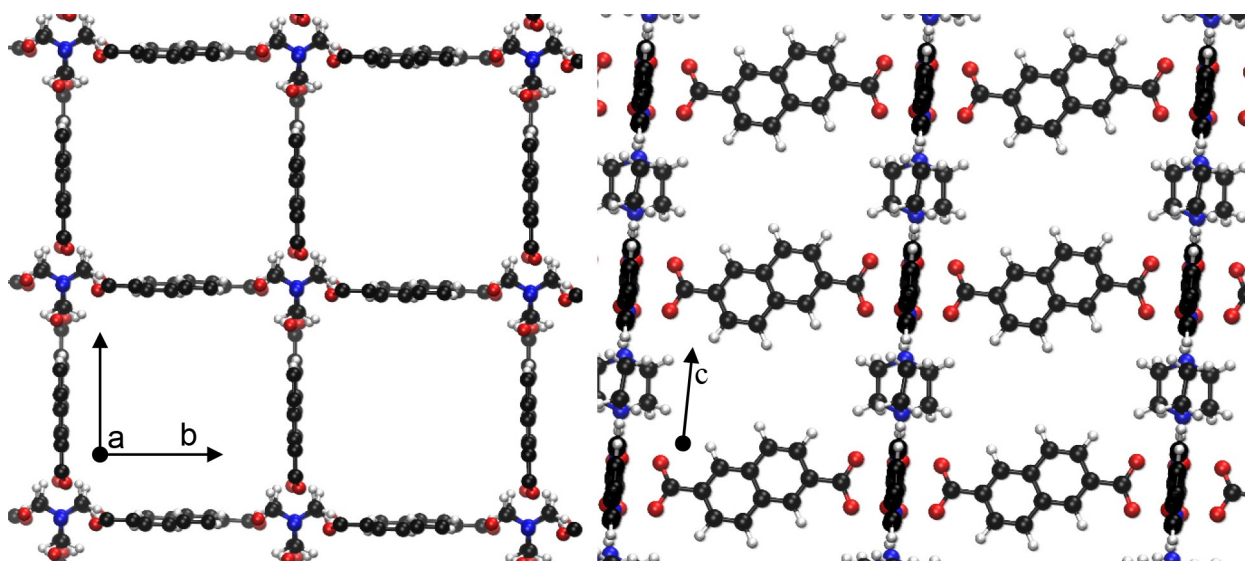


Figure 1. Graphical representation of DUT8-(Ni) conformer **B** in its open phase (**op**), viewed along the pillar axis (left, *c* axis) and along *ndc* linkers (right, *a* or *b* axis). Atoms colored by element: Nickel ochre, oxygen red, nitrogen blue, carbon black and hydrogen white. Reproduced under the terms of the Creative Commons Attribution 4.0 License.^[41] Copyright 2020, Zenodo.

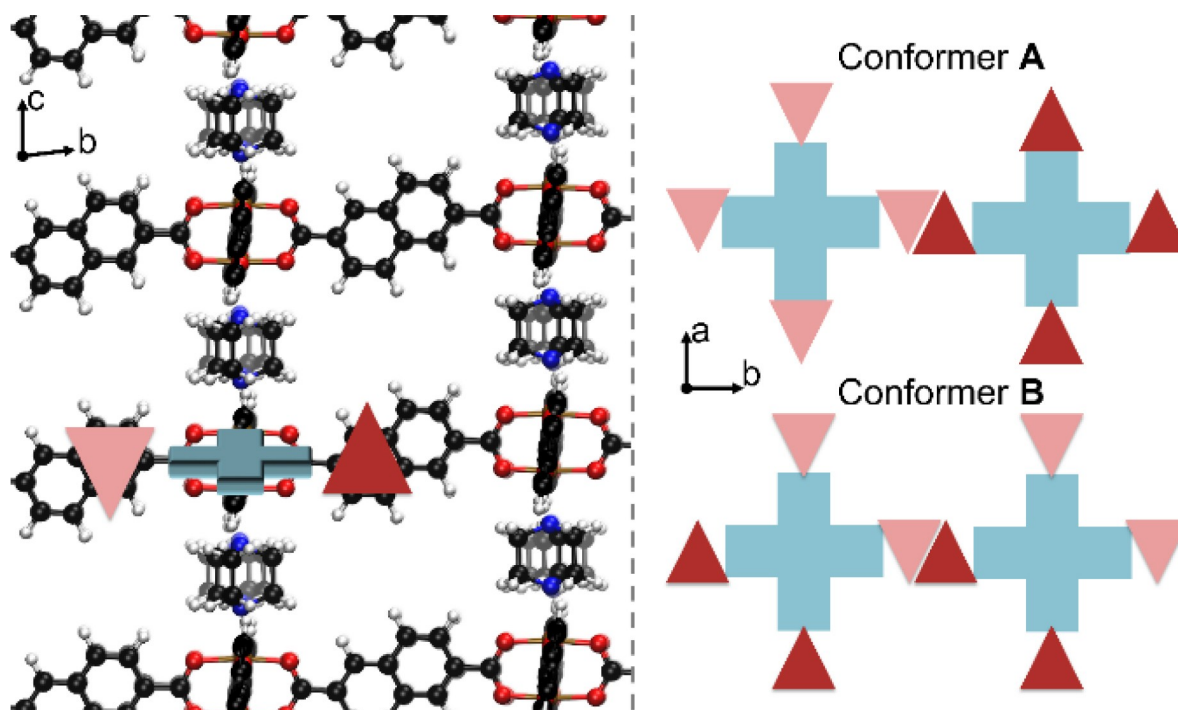


Figure 2. Graphical representation of DUT8-(Ni) conformer **B** in its open phase viewed along the *ndc* linkers (left). Schematic representation of linker orientations in the **A** and **B** conformer (right). Triangles represent a half *ndc* linker, either pointing up (dark red) or down (light red) with respect to the closest metal node (blue crosses). Reproduced under the terms of the Creative Commons Attribution 4.0 License.^[40] Copyright 2021, Zenodo.

the flexibility is not a unique characteristic of DUT-8(Ni) and has been observed and studied in other materials.^[21,22] Another important factor for the flexibility of DUT-8(Ni) is the exact conformation of the material. As shown previously, the non-linearity of the *ndc* linkers give rise to conformational isomerism.^[23] We showed that certain conformers result in a

specific stacking of the *ndc* linkers in the **cp** phase, increasing the dispersion interactions and therefore stabilizing it with respect to the **op** phase. Two relevant isomers were determined, an **A** conformer where all linkers of a paddle wheel point up or down, and a **B** conformer where opposing linkers on one paddlewheel point in opposite directions (see Figure 2).

Conformer **A** was found to be “rigid” (i.e. not transforming into the **cp** phase) in contrast to the “flexible” (i.e. transformation into **cp** is possible) conformer **B**. Recently, a more realistic modelling using nanodomains of differing conformers lead to an even better understanding of the real crystal system.^[24] The reverse transition of opening the structure from its **cp** phase to the **op** phase can be achieved by adsorbing guest molecules.^[18,20,23,25–33] Under the range of guest molecules able to reopen flexible DUT-8(Ni) are CO₂ and CH₄.

In a previous study of Sin *et al.*,^[30] the co-adsorption of CO₂ and CH₄ in rigid and flexible crystals of DUT-8(Ni) was studied by ¹³C NMR. The residual anisotropy (i.e. the line width of the NMR signal) of the ¹³C NMR signal of ¹³C labelled CO₂ can be directly related to the dynamic orientation of the CO₂ molecules.^[2,8] Sin *et al.* found that the residual chemical shift anisotropy of CO₂ is significantly smaller in the submicron-sized, rigid crystals than in the micrometer-sized, flexible crystals (see Figure 3). The measured ¹³C signal is for both rigid and flexible crystals much broader than in gaseous CO₂ (the gas peak is observed at approx. 126 ppm, see Figure 3), some dynamic order therefore remains even in the smallest crystals measured. This observation could back then not be attributed to a single cause, but two possible reasons were suggested: First, the smaller anisotropy could be caused by faster inter-particle exchange. Or second, the flexible framework could apply an ordering force onto the adsorbed CO₂ molecules that is not present in the rigid framework.^[30]

Using a line shape simulation methodology that has been successfully applied to MOFs,^[8] we can distinguish between these two possibilities. From molecular dynamics (MD) simulations we extract the trajectories of the adsorbed CO₂ molecules. We then calculate the residual chemical shift anisotropy (i.e. the chemical shift line width) based on these trajectories, following a previously published methodology^[8] that we implemented in a publicly available Python package.^[10] A similar methodology based on a different powder averaging algorithm was also published by Alavi *et al.* in 2008.^[9]

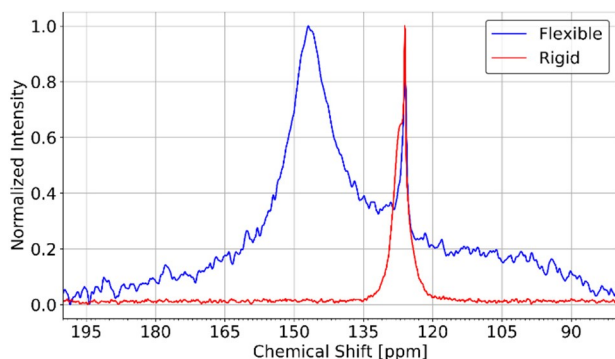


Figure 3. Measured ¹³C NMR spectra of CO₂ adsorbed in flexible (blue) and rigid (red) samples of DUT-8(Ni) at 215 K. Flexible sample measured at a partial CO₂ pressure of 5.1 bar (2:1 CO₂/CH₄ mixture, no CH₄ adsorption) and rigid sample measured at a CO₂ pressure of 6.6 bar. Both samples are in the **op** state at these experimental conditions. Adapted with permission from Sin *et al.*, Langmuir, 2019, 35 (8), 3162–3170. Copyright 2019 American Chemical Society.^[30]

Experimental Section

MD Simulations

We employ our previously published Ligand-Field Molecular Mechanics (LFMM) simulation setup for DUT-8(Ni).^[34,35] We perform three types of MD simulations: 1) CO₂ in the rigid **A** conformer of DUT-8(Ni) using a fully flexible cell (NσT ensemble); 2) CO₂ in the **B** conformer with a fully flexible cell (NσT ensemble); 3) CO₂ in the **B** conformer with a fixed cell (NVT ensemble, no restraints on atomic positions) in the **op** state. The simulation time of all simulations is 1 ns and temperatures of 200, 300 and 400 K are used for each of the three systems. For details of the LFMM parametrization see Ref. [34], further details of the MD simulations are given in Section 1.1 of the Supporting Information and adhere to the previous publications.^[34,35]

Line shape Simulation

In order to simulate the residual chemical shift anisotropy, we follow a slightly altered version of the calculation procedure published in ref.^[8] The theoretical background is presented in more detail in Section 1.2.1 of the Supporting Information, as it is thus far only completely available in German.^[36] It can shortly be described by the following procedure: For an anisotropic, linear molecule like CO₂, the shielding tensor σ contains two contributions, one for parallel (δ_{\parallel}) and one for perpendicular (δ_{\perp}) orientation to the external magnetic field B_0 . Since the chemical shifts δ of CO₂ for parallel and perpendicular orientation are known ($\delta_{\parallel} = -90$ ppm and $\delta_{\perp} = 245$ ppm, using TMS as Ref. [37]) and the chemical surrounding is anisotropic in only one spatial dimension, the chemical shift δ can be expressed as a function of only the orientation of the CO₂ molecule with respect to the external magnetic field B_0 .

The orientation of CO₂ molecules is approximated by the vector between the oxygen atoms (\vec{r}) and stored along the trajectory. All vectors are summed into a tensor – using the formula:

$$\sum_{i=1}^N \frac{\vec{r}_i \otimes \vec{r}_i}{r_i \cdot r_i},$$

where N represents the number of CO₂ molecules and \otimes denotes the dyadic product). This tensor represents the orientation of all molecules and can be calculated over any number of simulation steps. By diagonalizing this tensor and feeding it to a powder averaging algorithm (here the algorithm reported by Alderman *et al.*^[38] is used), relative line shapes can be calculated very efficiently (in a matter of minutes on any recent desktop or laptop computer). Spectra calculated by this procedure are with respect to a relative chemical shift Δ . This relative chemical shift Δ is equal to the chemical shift anisotropy (i.e. the line width of the NMR signal) of perfectly aligned, frozen CO₂, which is known to be $\Delta = \delta_{\perp} - \delta_{\parallel} = 335$ ppm.^[37] The linewidth of the calculated relative NMR signals can therefore directly be compared to the line width from experiment by multiplying it by $\Delta = 335$ ppm. As mentioned above, this approach is only valid when the host has a neglectable influence on the guests shielding tensor.

Details regarding the implementation are given in Section 1.2.2 of the Supporting Information.

Results and Discussion

For the two extreme cases of gaseous CO₂ (single peak of infinite height at $\bar{\delta}/\Delta = 2/3$, although a finite height and width arise from the numerical accuracy of the powder averaging algorithm) and perfectly aligned (i.e. frozen) CO₂ (line shape follows a functional dependence of $(4\sqrt{1 - \bar{\delta}/\Delta})^{-1}$) the calculated relative ¹³C NMR spectra can be visualized as shown in Figure 4. Simulations of CO₂ molecules exhibiting a partial ordering, like adsorbed CO₂ in DUT-8(Ni), yield a relative spectrum as the one given in Figure 4. The applicability of the method (a neglectable influence of the host on the shielding tensor of the guest) and the sampling have been validated as outlined in Section 1.2.3 and 1.2.4 of the Supporting Information. The relevant measure for comparison with experimental

data is the width of the calculated spectra. In the example given in Figure 4, this amounts to approximately 0.1 which is equal to a residual shift anisotropy (i.e. a line width) of 33.5 ppm. To assert the validity of the observed line widths, we calculated the instantaneous temperature of the MOF, the guest molecules and the entire system based on the final atomic velocities. The resulting temperatures are given in Section 2.2 of the Supporting Information. No significant deviation from the set thermostat temperature is observed.

The accumulated relative line widths of the rigid and flexible cell simulations with respect to the loading are given in Figure 5 (the corresponding plot of simulations of the A conformer are given in Figure S15 of the Supporting Information). All calculated line shapes are given in Sections 2.4 to 2.6 of the Supporting Information. Low loadings in the flexible simulation cell (right panel of Figure 5) exhibit a high ordering

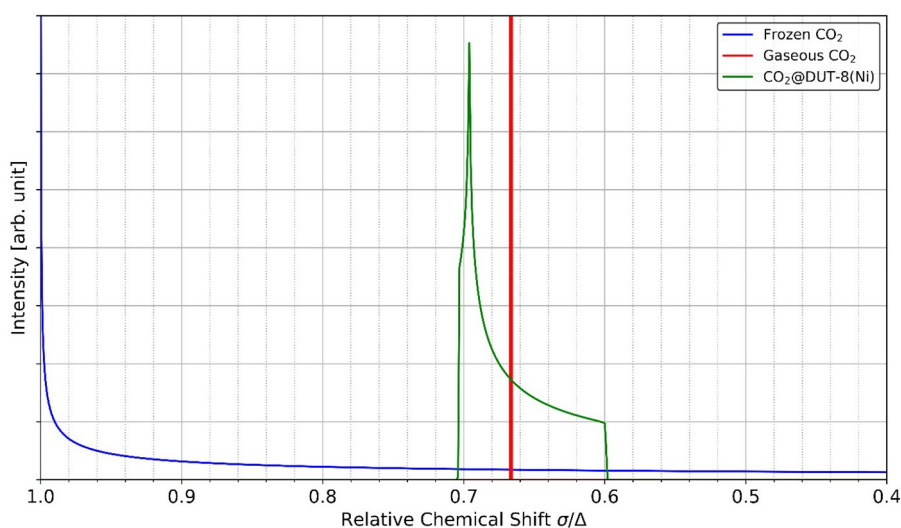


Figure 4. Calculated relative ¹³C NMR spectra for perfectly aligned, frozen CO₂ (blue), gaseous CO₂ (red) and an exemplary result from our simulations (green). The example given is the result from our rigid cell 400 K simulation with 18 molecules of CO₂. Reproduced under the terms of the Creative Commons Attribution 4.0 License.^[40] Copyright 2021, Zenodo.

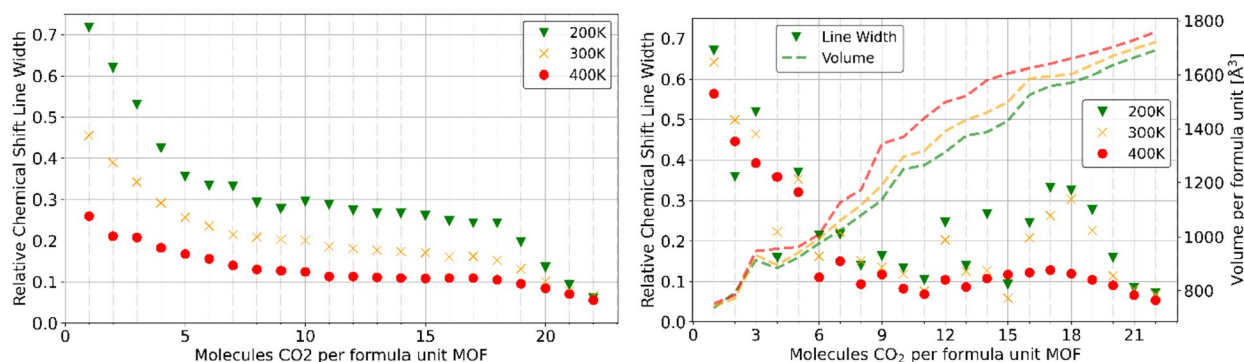


Figure 5. Relative chemical shift line widths with respect to the number of CO₂ molecules loaded per formula unit MOF at 200 K (green), 300 K (yellow) and 400 K (red) simulation temperature. Left: rigid cell simulations of the B conformer in the op state. Right: Flexible cell simulations of B conformer, cell volumes given as dashed lines. Experimentally, the maximum loading is expected to be in the range of 18 to 22 molecules per formula unit MOF (see text). Reproduced under the terms of the Creative Commons Attribution 4.0 License.^[40] Copyright 2021, Zenodo.

(large line width) across all temperatures, as the closed framework confines the few adsorbed CO₂ molecules. In the rigid cell (left panel of Figure 5, same volume as the fully loaded flexible cell at the corresponding temperature), low loadings exhibit more CO₂ movement than in the flexible cell for simulation temperatures above 200 K. This is to be expected since the confinement by the framework is much less intense (larger pores). Since the first molecules to be adsorbed have access to the strongest adsorption sites, they however still exhibit a high degree of order resulting in almost “frozen” positioning at lower temperatures. Increasing the simulation temperature counteracts the adsorption energy and leads to a higher mobility of the adsorbate. In the flexible simulations (right panel of Figure 5), however, the confining influence at low loadings is the framework. Raising the temperature therefore does not significantly affect the mobility of the guest. Only at higher loadings, when the MOF is already significantly opened, the mobility of the guest differs between simulation temperatures. At the maximum simulated loading of 22 molecules, neither temperature nor flexibility of the host play a significant role since the packing of CO₂ is dense and liquid-like (meaning no pronounced preferential ordering). The experimental maximum loading is difficult to determine exactly. As shown by Bon *et al.*,^[27] even after adsorption some parts of the MOF stay closed. By estimating the relative amount of closed MOF one can derive a theoretical maximum loading of 21.5 molecules per formula unit MOF. As this requires *in situ* XRD measurements, this is not commonly done. The maximum loadings of CO₂ in DUT-8(Ni) published therefore differ quite significantly.^[17,26,27,30] From our previous simulations^[34] and the experimental results mentioned, we suggest that the maximum loading in experiments will be in the range of 18 to 22 molecules CO₂ per formula unit MOF (i.e. 27.36 to 33.45 mmol/g). The simulated line widths in this regime are close to 0.1 for temperatures of 300 K and 400 K for the simulations of the rigid variant as well as for the flexible one (see Figure 5). A significant increase in alignment of the CO₂ molecules is therefore not observed in the flexible framework compared to the rigid one at full loading. The simulations therefore do not support the explanation of the residual chemical shift anisotropy by a framework-induced force on the adsorbates in the flexible samples. Since the simulation of micrometer sized crystals is well beyond the computationally accessible simulation size regimes, we are bound to the periodic boundary approximation. It is therefore not possible to provide computational proof of the first explanation (fast interparticle exchange). We can only argue against the second explanation via an ordering force applied by the framework. An exemplary comparison of experimental and calculated line shapes is presented in Figure S20 in the Supporting Information. The observed line width of 0.1 (equals 33.5 ppm), however, perfectly agrees with the measured line widths in the flexible crystals of Sin *et al.*^[30] We therefore propose multiple hypotheses: First, the difference in line width in the rigid crystals could be due to differences in the inter-particle exchange, as already suggested by Sin *et al.*^[30] This should be experimentally observable by varying pressure and crystallite

sizes (inside the rigid size regime). Secondly, the difference in line width could also be due to different defect concentrations. EPR studies of DUT-8 have previously shown, that the rigid and flexible crystals also exhibit different defect concentrations.^[20] It is imaginable that the higher mobility of guests at defect sites due to reduced confinement is the cause of the decreased line width.

Conclusions

Through theoretical calculations of ¹³C NMR line widths from MD simulations, we have disproven a possible reason for the difference in residual chemical shift anisotropy of the ¹³C NMR signal of carbon dioxide in rigid and flexible forms of DUT-8(Ni). The lower anisotropy (narrower signal) of CO₂ in the rigid DUT-8(Ni) samples can, according to our simulations, not be explained by an ordering force of the framework on the carbon dioxide molecules. The flexibility of the framework does not influence the orientation of the guest molecules at full loading and can therefore not be the cause of the broader signal (higher degree of order) in the flexible, larger crystallites. The methods and tools used throughout this work are not specific to the investigated MOF and can therefore be used to study confinement of CO₂ in other materials. By implementing a fast and easy to use algorithm, we enable a wide community to perform direct comparisons between NMR measurements and MD simulation.

Supporting Information

Supporting Information is available online. All input/output, scripts, structures, plots etc. of the simulations are published as raw data (and visualizations thereof).^[39–41]

The NMR line shape simulation software developed and used throughout this work is available online.^[10]

Author Contributions

P.M. ran MD simulations and wrote the line shape simulation software. T.H. contributed to the analysis of the MD simulations by providing ideas for the analysis. P.M. prepared the manuscript and the review process. T.H. acquired the relevant funding and contributed ideas to the manuscript.

Acknowledgements

This work was funded by DFG through FOR2433. PM acknowledges funding by the Humboldt foundation through a Feodor-Lynen fellowship during writing of this article. We thank ZIH Dresden for providing computational resources. We gratefully acknowledge the fruitful discussions with Dr. S. Ehrling, M. Rauche and especially Prof. E. Brunner, who initiated the investigation and provided insights, experimental data and feedback for the manu-

script. Open Access funding enabled and organized by Projekt DEAL.

Conflict of Interest

The authors declare no conflict of interest.

Keywords: NMR · metal-organic frameworks · molecular dynamics · DUT-8 · CO₂ · line shape

- [1] E. Brunner, M. Rauche, *Chem. Sci.* **2020**, *11*, 4297–4304.
- [2] V. J. Witherspoon, J. Xu, J. A. Reimer, *Chem. Rev.* **2018**, *118*, 10033–10048.
- [3] Y. T. A. Wong, V. Martins, B. E. G. Lucier, Y. Huang, *Chem. Eur. J.* **2019**, *25*, 1848–1853.
- [4] X. Kong, E. Scott, W. Ding, J. A. Mason, J. R. Long, J. A. Reimer, *J. Am. Chem. Soc.* **2012**, *134*, 14341–14344.
- [5] Y. Zhang, B. E. G. Lucier, Y. Huang, *Phys. Chem. Chem. Phys.* **2016**, *18*, 8327–8341.
- [6] Y. Lu, B. E. G. Lucier, Y. Zhang, P. Ren, A. Zheng, Y. Huang, *Phys. Chem. Chem. Phys.* **2017**, *19*, 6130–6141.
- [7] R. M. Marti, J. D. Howe, C. R. Morelock, M. S. Conradi, K. S. Walton, D. S. Sholl, S. E. Hayes, *J. Phys. Chem. C* **2017**, *121*, 25778–25787.
- [8] V. Bon, J. Pallmann, E. Eisbein, H. C. Hoffmann, I. Senkovska, I. Schwedler, A. Schneemann, S. Henke, D. Wallacher, R. A. Fischer, et al., *Microporous Mesoporous Mater.* **2015**, *216*, 64–74.
- [9] S. Alavi, P. Dornan, T. K. Woo, *ChemPhysChem* **2008**, *9*, 911–919.
- [10] P. Melix **2019** *NMR Lineshape*, Zenodo, DOI 10.5281/zenodo.3450684.
- [11] C. Serre, F. Millange, C. Thouvenot, M. Noguès, G. Marsolier, D. Louër, G. Férey, *J. Am. Chem. Soc.* **2002**, *124*, 13519–13526.
- [12] M. Eddaoudi, *Science* **2002**, *295*, 469–472.
- [13] S. Kitagawa, R. Kitaura, S. Noro, *Angew. Chem. Int. Ed.* **2004**, *43*, 2334–2375; *Angew. Chem.* **2004**, *116*, 2388–2430.
- [14] G. Férey, C. Serre, *Chem. Soc. Rev.* **2009**, *38*, 1380–1399.
- [15] A. Schneemann, V. Bon, I. Schwedler, I. Senkovska, S. Kaskel, R. A. Fischer, *Chem. Soc. Rev.* **2014**, *43*, 6062–6096.
- [16] H. Li, M. Eddaoudi, M. O’Keeffe, O. M. Yaghi, *Nature* **1999**, *402*, 276–279.
- [17] N. Klein, C. Herzog, M. Sabo, I. Senkovska, J. Getzschmann, S. Paasch, M. R. Lohe, E. Brunner, S. Kaskel, *Phys. Chem. Chem. Phys.* **2010**, *12*, 11778–11784.
- [18] N. Kavooosi, V. Bon, I. Senkovska, S. Krause, C. Atzori, F. Bonino, J. Pallmann, S. Paasch, E. Brunner, S. Kaskel, *Dalton Trans.* **2017**, *46*, 4685–4695.
- [19] J. Y. Lee, L. Pan, X. Huang, T. J. Emge, J. Li, *Adv. Funct. Mater.* **2011**, *21*, 993–998.
- [20] M. Mendt, F. Gutt, N. Kavooosi, V. Bon, I. Senkovska, S. Kaskel, A. Pöpl, *J. Phys. Chem. C* **2016**, *120*, 14246–14259.
- [21] S. M. J. Rogge, M. Waroquier, V. van Speybroeck, *Nat. Commun.* **2019**, *10*, 4842.
- [22] J. Keupp, R. Schmid, *Adv. Theory Simul.* **2019**, *2*, 1900117.
- [23] P. St. Petkov, V. Bon, C. L. Hobday, A. B. Kuc, P. Melix, S. Kaskel, T. Düren, T. Heine, *Phys. Chem. Chem. Phys.* **2019**, *21*, 674–680.
- [24] S. Ehrling, E. M. Reynolds, V. Bon, I. Senkovska, T. E. Gorelik, J. D. Evans, M. Rauche, M. Mendt, M. S. Weiss, A. Pöpl, E. Brunner, U. Kaiser, A. L. Goodwin, S. Kaskel, *Nat. Chem.* **2021**, *13*, 568–574.
- [25] H. C. Hoffmann, B. Assfour, F. Epperlein, N. Klein, S. Paasch, I. Senkovska, S. Kaskel, G. Seifert, E. Brunner, *J. Am. Chem. Soc.* **2011**, *133*, 8681–8690.
- [26] N. Klein, H. C. Hoffmann, A. Cadiau, J. Getzschmann, M. R. Lohe, S. Paasch, T. Heydenreich, K. Adil, I. Senkovska, E. Brunner, S. Kaskel, *J. Mater. Chem.* **2012**, *22*, 10303–10312.
- [27] V. Bon, N. Klein, I. Senkovska, A. Heerwig, J. Getzschmann, D. Wallacher, I. Zizak, M. Brzhezinskaya, U. Mueller, S. Kaskel, *Phys. Chem. Chem. Phys.* **2015**, *17*, 17471–17479.
- [28] A. Krylov, A. Vtyurin, P. Petkov, I. Senkovska, M. Maliuta, V. Bon, T. Heine, S. Kaskel, E. Slyusareva, *Phys. Chem. Chem. Phys.* **2017**, *19*, 32099–32104.
- [29] M. Mendt, S. Ehrling, I. Senkovska, S. Kaskel, A. Pöpl, *Inorg. Chem.* **2019**, *58*, 7, 4561–4573.
- [30] M. Sin, N. Kavooosi, M. Rauche, J. Pallmann, S. Paasch, I. Senkovska, S. Kaskel, E. Brunner, *Langmuir* **2019**, *35*, 3162–3170.
- [31] H. Miura, V. Bon, I. Senkovska, S. Ehrling, S. Watanabe, M. Ohba, S. Kaskel, *Dalton Trans.* **2017**, *46*, 14002–14011.
- [32] S. Ehrling, I. Senkovska, V. Bon, J. D. Evans, P. Petkov, Y. Krupskaya, V. Kataev, T. Wulf, A. Krylov, A. Vtyurin, S. Krylova, S. Adichtchev, E. Slyusareva, M. S. Weiss, B. Büchner, T. Heine, S. Kaskel, *J. Mater. Chem. A* **2019**, *7*, 21459–21475.
- [33] M. Rauche, S. Ehrling, S. Krause, I. Senkovska, S. Kaskel, E. Brunner, *Chem. Commun.* **2019**, *55*, 9140–9143.
- [34] P. Melix, F. Paesani, T. Heine, *Adv. Theory Simul.* **2019**, *2*, 1900098.
- [35] P. Melix, T. Heine, *J. Phys. Chem. C* **2020**, *124*, 11985–11989.
- [36] E. Eisbein Molekulardynamische Simulationen zu Wirt-Gastsystemen auf der Basis von Metallorganischen Gerüstverbindungen. TU Dresden. Phdthesis.
- [37] A. J. Beeler, A. M. Orendt, D. M. Grant, P. W. Cutts, J. Michl, K. W. Zilm, J. W. Downing, J. C. Facelli, M. S. Schindler, W. Kutzelnigg, *J. Am. Chem. Soc.* **1984**, *106*, 7672–7676.
- [38] D. W. Alderman, Mark S. Solum, David M. Grant, *J. Chem. Phys.* **1986**, *84*, 3717–3725.
- [39] P. Melix **2019** A Ligand Field Molecular Mechanics Study of CO₂ Induced Breathing in the metal-organic framework DUT-8(Ni), Zenodo, DOI 10.5281/zenodo.2808647.
- [40] P. Melix **2021** Investigation of CO₂ Orientational Dynamics through Simulated NMR Line Shapes, Zenodo, DOI 10.5281/zenodo.4905822.
- [41] P. Melix **2020** London Dispersion Governs the Interaction Mechanism of Small Polar and Non-Polar Molecules in Metal-Organic Frameworks, Zenodo, DOI 10.5281/zenodo.3631181.

Manuscript received: June 25, 2021
Revised manuscript received: August 31, 2021
Accepted manuscript online: September 6, 2021
Version of record online: September 23, 2021